Heliyon 11 (2025) e42546

Contents lists available at ScienceDirect

Heliyon

journal homepage: www.cell.com/heliyon

Research article

Application of cellulose/poly(vinylidene fluoride) blend films as polymer electrolytes in lithium ion batteries

Shirin Mohamadzade [a,b,1], Seyedeh-Arefeh Safavi-Mirmahalleh [a,b,1], Hossein Roghani-Mamaqani [a,b], Mehdi Salami-Kalajahi [a,b,*]

[a] Faculty of Polymer Engineering, Sahand University of Technology, P.O. Box 51335-1996, Tabriz, Iran
[b] Institute of Polymeric Materials, Sahand University of Technology, P.O. Box 51335-1996, Tabriz, Iran

ARTICLE INFO

Keywords:
Polymer blends
Polymer electrolyte
Cellulose
poly(vinylidene fluoride)
Lithium-ion battery

ABSTRACT

Polymer electrolytes are the most promising replacement for liquid electrolytes in lithium ion batteries (LIBs) due to their unique properties. Beside this, polymer blends are usually used as polymer electrolytes to achieve expectable properties including properties of each component. In this study, cellulose/poly(vinylidene fluoride) (PVDF) blend films are prepared *via* solution casting at different weight ratios. To investigate phase behavior of binary system, the thermodynamic interaction parameter of Flory-Huggings is evaluated. The X-ray diffraction spectroscopy (XRD) analysis is conducted to investigate the structural properties of samples. Differential scanning calorimetry (DSC) and thermogravimetric analysis (TGA) analyses were performed to study thermal behaviors. Mechanical properties are investigated by tensile test and electrochemical properties such as electrochemical impedance spectroscopy (EIS), linear sweep voltammetry (LSV), and chronoamperometry are studied. The results and morphology of these blends showed phase separation of two polymers. This phase separation led to the creation of free volume, which is a path for ion transfer; therefore, the ion conductivity was obtained in the range of 10^{-4} S cm^{-1}. In addition, high transfer number ($0.41 < t^{+} < 0.97$), wide electrochemical stability window (>5 V), acceptable charge capacity (>200 mAh/g at 0.2C), and long cycle stability was achieved.

1. Introduction

With the rapid development of the energy storage industry, lithium-ion batteries (LIBs) with the advantages of lightweight, high-energy density, fast charging, and low self-discharge have recently dominated the market of portable electronic devices such as laptops, mobile phones, and cameras [1,2]. To address safety issues such as dendrite growth, combustion, and organic solvent leakage in traditional LIBs with liquid electrolytes, solid-gel polymer electrolytes have garnered attention. These alternatives offer improved safety, reduced weight, flexibility, and shape versatility [3–6]. Polymer electrolytes based on synthetic polymers such as poly(ethylene oxide) (PEO), polyacrylonitrile (PAN), poly(methyl methacrylate) (PMMA), poly(dimethyl siloxane) (PDMS), and poly(vinylidene fluoride) (PVDF) lead to severe environmental pollution so, the utilization of renewable polymers results in more environmentally friendly LIBs [7,8].

* Corresponding author. Faculty of Polymer Engineering, Sahand University of Technology, P.O. Box 51335-1996, Tabriz, Iran.
E-mail addresses: m.salami@sut.ac.ir, m.salamikalajahi@gmail.com (M. Salami-Kalajahi).
[1] Both authors have contributed equally as first authors.

https://doi.org/10.1016/j.heliyon.2025.e42546
Received 17 September 2024; Received in revised form 5 February 2025; Accepted 7 February 2025
Available online 7 February 2025

Cellulose stands out as the most promising natural polymer due to its hydrophilicity, excellent physical properties, chemical and thermal stability, and numerous electron donor groups in its structure, which facilitate the dissolution of lithium salts. The main drawback of high T_g and low mechanical strength limit its further use alone [9–11]. Polymer blends, composed of structurally and functionally diverse polymers, are ideal for use in LIBs due to their feasibility, cost-effectiveness, and novel functionalities. From a thermodynamic perspective, polymer blends are classified as either miscible or immiscible [12–15]. To circumvent the issue of cellulose, PVDF can be a good candidate to blend with cellulose because of low T_g, high dielectric constant, considerable electrochemical stability, and mechanical strength [16,17]. In this regard, Zhang et al. prepared a porous and honeycomb-structured cellulose and PVDF membranes as gel polymer electrolytes (GPEs) in different weight ratios and these membranes showed properties such as high ion conductivity (1.89 mS cm^{-1}), high transfer number up to 0.89, and good electrochemical stability (5.35 V) [18]. A blend of GPEs containing ethyl cellulose/PVDF in different ratios which revealed high ionic conductivity and lithium ion transfer number were prepared by Nan et al. [19]. Zhang et al. have prepared a GPE based on PVDF/hydroxyethyl cellulose (HEC)/PVDF membrane with high ion conductivity, lithium transfer number, and wide electrochemical window [20].

In this work, cellulose derived from Whatman paper as sustainable natural material is blended with PVDF to prepare a series of films with varying weight ratios by using solution casting technique. Afterward, thermodynamically, the phase separation of these films is investigated by Flory-Huggins theory. These thermodynamic principles of miscibility have been demonstrated to have an effect not only on morphological, thermal, and physical features but also on the electrochemical performance of blend polymer electrolytes. The results showed that blend electrolytes had high ionic conductivity, great lithium transfer number, and outstanding charge-discharge capacity. When the cellulose to PVDF ratio is 90/10 and 80/20, electrochemical properties achieve an optimal value.

2. Experimental section

2.1. Materials

Whatman No. 1 filter paper was used as the cellulose substrate due to its high cellulose content, containing 98 % α-cellulose, and minimal impurities. Molecular weight of cellulose was ~400,000 g/mol. Ethanol (Merck, 99.8 %), sodium hydroxide (NaOH, Sigma-Aldrich, 98 %), dimethyl sulfoxide (DMSO, Sigma-Aldrich, 99.5 %), lithium hexafluorophosphate ($LiPF_6$, Sigma-Aldrich, 99.99 %), dimethyl carbonate (DMC, Sigma-Aldrich, 99 %), diethyl carbonate (DEC, Sigma-Aldrich, 99 %), poly(vinylidene fluoride) (PVDF, molecular weight ~ 534,000 g/mol, Sigma-Aldrich), lithium cobalt(III) oxide ($LiCoO_2$, Sigma-Aldrich, 99.8 %), carbon black (Sigma-Aldrich, 99.95 %), *N*-methyl-2-pyrrolidone (NMP, Sigma-Aldrich, 99.5 %), and graphite (Sigma-Aldrich) were used as received.

2.2. Preparation of cellulose

Whatman paper was chopped and washed with ethanol. To break down the extension hydrogen bonding between OH groups of cellulose and open up the ordered regions, these chopped papers were added to NaOH/distilled water (10 g/100 mL) and stirred for 72 h at room temperature. To obtain a neutral mixture, the samples were washed repeatedly with ethanol. Finally, the resulting product was freeze-dried.

2.3. Blending of PVDF and cellulose

Cellulose and PVDF with different weight ratios (cellulose/PVDF) (0/100 (P_{10}), 50/50 (C_5P_5), 60/40 (C_6P_4), 70/30 (C_7P_3), 80/20 (C_8P_2), 90/10 (C_9P_1), and 100/0 (C_{10})) were mixed individually with dimethyl sulfoxide (DMSO). Then, two mixtures were combined together at room temperature until a homogeneous system was obtained. The mixture was casted in a Teflon mold and solvent was evaporated at 60 °C in a vacuum oven for 48 h.

2.4. Preparation of electrolyte films

The polymer electrolytes were obtained by swelling the blend films in a 1 M solution of $LiPF_6$ in diethyl carbonate (DEC)/dimethyl carbonate (DMC) (1:1 v/v) for 48 h and then used for further measurements.

2.5. Preparation of cathode and anode

The cathode comprised 80 *wt* % $LiCoO_2$ (active material), 5 *wt* % PVDF (binder), and 15 *wt* % carbon black (conductive additive), while the anode consisted of 80 *wt* % graphite (active material), 5 *wt* % PVDF (binder), and 15 *wt* % carbon black (conductive additive). These components were suspended in NMP and coated onto aluminum foil for the cathode and Cu sheet for the anode. The coated sheets were vacuum-dried at 80 °C for 24 h. All cell preparations and electrochemical analyses were conducted in a glovebox filled with N_2 gas. Polymer electrolytes (~30 mm^2 in area and ~0.5 mm in thickness) were sandwiched between the cathode and anode.

2.6. Characterizations

The morphology of films was studied using a Tescan MIRA5 FE-SEM. Before analysis, the electrolytes were freeze-dried, and liquid nitrogen was used to break the blend films. The samples were subsequently coated with gold. A thermal gravimetric analyzer (Polymer

Laboratories, TGA 1000, UK) was applied for studying thermal stability. The samples were heated from room temperature to 800 °C at a rate of 10 °C/min in an atmosphere of nitrogen. The samples weighed ~10 mg. Differential scanning calorimeter (NETZSCH DSC 200 F3, Netzsch Co., Bavaria, Germany) was used to study the thermophysical behavior of the films. About 10 mg of the material was put in an aluminum pan and tested at temperatures ranging from −90 to 220 °C with a heating rate of 10 °C/min in a nitrogen environment. The following formula was used to calculate the crystallinity (X_c) from the DSC curves.

$$X_C = \frac{\Delta H_m}{\Delta H_{m^\circ} \times \varphi} \times 100 \quad (1)$$

An X-ray diffractometer (Siemens, Germany D5000) was utilized to determine crystallinity. The test used an X-ray source Cu kα (λ = 0.1540 nm) with a 2θ angle of 10–80°. Mechanical properties were tested using a tensile test. This test was performed based on the ASTM D 638M − 3 standard (German Z010 machine-Zwick/Roll). First, dumbbell-shaped samples were prepared from the films and stretched at a constant rate of 10 mm/min. The electrolyte uptake ratio was determined by swelling after soaking in EMC/DMC (1:1 v/v) at varying time intervals. Equation (2) was employed for calculating the electrolyte uptake, also which is referred to AS%.

$$AS\% = \frac{W_t - W_0}{W_0} * 100 \quad (2)$$

Here W_t and W_0 represent the weights of the films after and before electrolyte absorption.

2.7. Electrochemical characterizations

The ionic conductivity has been studied utilizing electrochemical impedance spectroscopy. Two stainless steel electrodes were employed, with the electrolyte placed between them. The Potentiostat Galvanostat-PGE 18 (IRASOL) was utilized with a voltage of 10 mV and a frequency of 0.1 Hz–1 MHz. The ionic conductivity was estimated using Equation (3). The temperature-dependent ionic conductivity was calculated in the temperature range of 25–55 °C.

$$\sigma = \frac{h}{R_b A} \quad (3)$$

where σ is the value of the ionic conductivity (S cm^{-1}), h indicates the thickness of the GPE (cm), R_b is the bulk resistance (Ω), and A is the electrode/electrolyte interface area (cm^2).

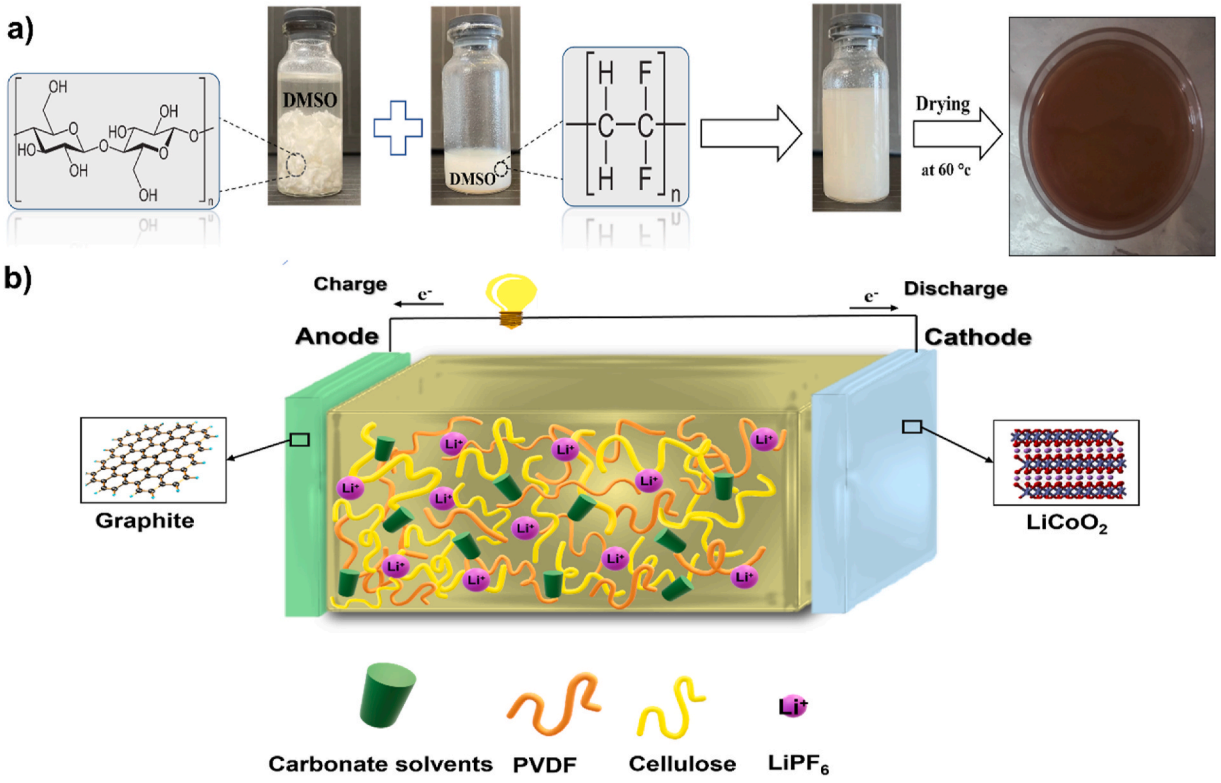

Fig. 1. a) Preparation of blend films, b) Cell assembly using polymer electrolytes.

The transference number (t^+) of GPEs was calculated using Evans, Vincent, and Bruce's potentiostatic polarization approach. Electrolytes were sandwiched in a symmetric cell of Gr/electrolyte/Gr and conducted at a constant potential of 5 mV. The transference number (t^+) of electrolytes was estimated using a combination of chronoamperometry and EIS, according to Equation (4):

$$t_{Li}^{+} = \frac{I_{ss}\,(\Delta V - I_0\,R_0)}{I_0(\Delta V - I_{ss}\,R_{ss})} \tag{4}$$

In this equation, I_0, I_{ss}, R_0, and R_{ss} indicate the initial constant current, the current after reaching the steady state, the initial resistance and the final resistance, respectively.

A cyclic voltammetry test was performed utilizing the PGE (IRAS01) device in the potential range of 1–5 V in order to verify the electrochemical stability window. The electrolytes were sandwiched between the stainless steel and the anode to perform the test. The galvanostatic charge and discharge (constant current) cycling experiments were done at room temperature on a $LiCoO_2$/GPE/Gr in the potential window of 2.5–5 V at various current rates of 0.1, 0.2, 0.5, and 1 C with an Atomlab electrochemical workstation. The galvanostatic charge/discharge cycling performance of GPEs on $LiCoO_2$/GPE/Gr cells was also examined for 100 cycles at 0.2 C.

3. Results and discussion

Cellulose and PVDF were blended at different weight ratios *via* solution casting method. These films were swelled in lithium salt solution and then used as polymer electrolytes of LIB cells. Fig. 1a shows the graphical depiction of the cellulose/PVDF blend preparation and Fig. 1b shows cell assembly of prepared polymer electrolytes.

3.1. Characterization of blend films

The immiscibility of PVDF and cellulose was investigated under general thermodynamic framework, using Equations (S1)-(S4) (Section S1, Supporting **Information**), and the results are presented in Table 1. The lower value of $\chi_{critical} = 0.000512$ than χ of films reported in Table 1 indicates that cellulose and PVDF are thermodynamically immiscible and give phase separation in all blend compositions. The values of χ and δ increased as the cellulose content increased in blend films and more phase separation occurred. To identify the effect of phase separation on morphology, Fig. 2 depicts the FE-SEM results. Samples C_5P_5 and C_6P_4 have the most dispersed phase, the two polymers are partially dispersed in each phase. Furthermore, the phase separation of PVDF phase leads to aggregation of PVDF as dispersed phase and fewer pores are also seen. In C_7P_3 sample, further phase separation of dispersed phase have occurred and the two polymers have formed separate phases and this has led to closing the pores. C_8P_2 and C_9P_1 show the most phase separation based on interaction parameters which was consistent with the morphology. This phase separation leads to the creation of holes and free volume [21].

Thermal stability of blend films and swollen electrolytes is analyzed by TGA (Fig. 3a and Table S1). The blend films showed weight loss above 350 °C corresponding to cellulose decomposition, and another weight loss occurred above 400 °C which refers to the PVDF decomposition. The resulting two-stage decomposition is due to the immiscibility of two polymers. In swollen samples, the first stage weight loss between 100 and 200 °C is attributed to the evaporation of organic solvent. It can be observed that $T_{d,5\ \%}$ (the temperature of 5 % weight loss) of swollen films showed a decrease compared to blend films before swelling due to volatile carbonate molecules. The decomposition temperature of cellulose and PVDF shifted slightly to a higher value. The DSC measurement was used to study the thermal behavior of blend films (Fig. 3b and Table S1). The observed endothermic peak in blend films assigned to the melting of the crystalline structure of PVDF. By increasing cellulose content (50–90 %), melting temperature decreased slightly from 165.7 to 157.3 °C and the crystallinity (calculated by Equation (1)) decreased from 50.0 to 11.9 %. This change can be explained by the formation of more free volume that was created from phase separation arising from the immiscibility of two polymers. This free volume leads to facilitating the segmental motion of the polymer chains making the polymer chain tangled and folded more easily. The glass transition temperature (T_g) of cellulose was observed at 52.1 °C, whereas that of PVDF was at −40.8 °C. The significantly higher T_g value of cellulose can be attributed to the strong hydrogen bonding between its chains, which restricts molecular mobility and thus requires more thermal energy to achieve the glass transition. For the blended films, no distinct T_g peak was observed. This absence may be due to the scan rate used during the measurement; a faster scan rate can sometimes obscure the detection of the T_g, especially if the transition is broad or if the interaction between the polymers affects the sharpness of the T_g signal.

XRD patterns of prepared films are displayed in Fig. 3c and the degree of crystallinity is reported in Table S1 α, β, γ, and δ are the

Table 1
Hansen solubility parameters and Flory-Huggins interaction parameters of the pure polymers and blend films.

Samples	δ_d (Mpa ½)	δ_p(Mpa ½)	δ_H (Mpa ½)	Reference	Δδ (Mpa ½)	χ_{12}
P_{10}	17.2	12.5	9.2	22	23.2	–
C_5P_5	20.8	13.7	20.1	–	32.0	0.029
C_6P_4	21.5	13.9	22.2	–	33.9	0.035
C_7P_3	22.0	14.2	24.4	–	36.0	0.045
C_8P_2	23.0	14.4	26.6	–	37.9	0.054
C_9P_1	23.7	14.7	28.7	–	40.1	0.065
C_{10}	24.4	14.9	30.9	22	42.1	–

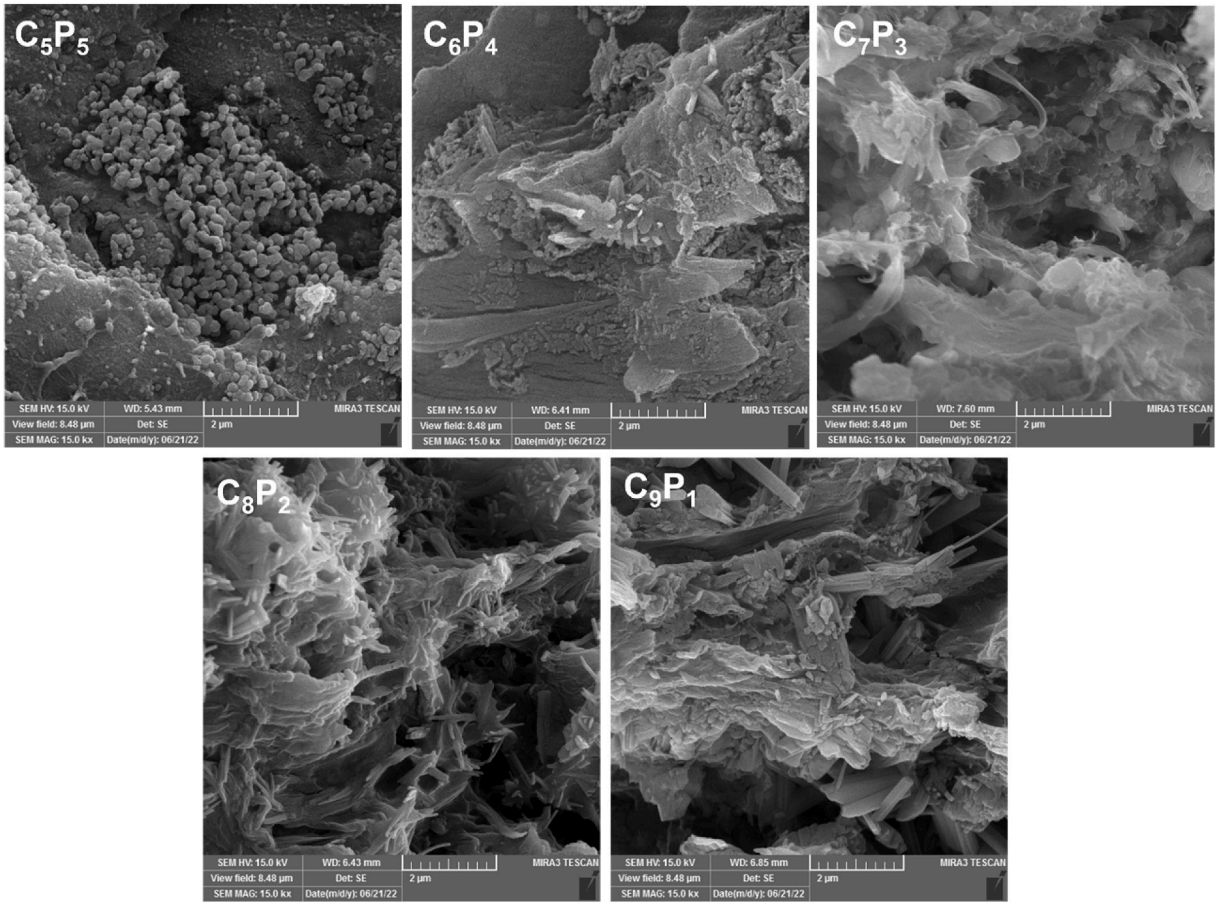

Fig. 2. FE-SEM images of the blend films (C_5P_5-C_9P_1) with different PVDF/Cellulose weight ratios.

crystal phases of PVDF that arise from the different chain conformations. Among these polymorphs, α and β are the most common, whereas the β phase crystal has an effective role in improving ionic conductivity due to its polar structure [22]. As shown in XRD patterns, the peaks at 2θ equal to 14.9, 16.7, and 20.3° are corresponding characteristic diffraction peaks of cellulose [23,24]. The pristine PVDF displays peaks at 18.1 and 39.7°, corresponding to the α-phase crystal, while the β-phase crystal peak appears at 20.7° [25]. After blending, similar peaks were observed at different compositional ratios, also the intensity of PVDF peaks weakened by decreasing the amount of PVDF in blend films. Overlapping of PVDF and cellulose peaks in blends impedes estimation of the relative fraction of β phase crystals however increment of cellulose content led to preferential formation of β phase which is correlated to heterogeneous crystallization of PVDF chain on the surface of cellulose [26]. It can be noted that the degree of crystallinity of blends decreases from 50.7 to 44.9 % by increasing the cellulose content from 50 to 90 %. The sharper peaks in cellulose primarily result from its inherent crystalline structure, but the overall crystallinity in the polyblends is influenced by phase separation and interaction dynamics between cellulose and PVDF. When phase separation is prominent, each phase retains its own crystalline nature, allowing distinct peaks to persist. However, if interaction increases between the phases, crystallinity may reduce due to disruption of ordered folding in polymer chains, without necessarily leading to co-crystallization [26].

Prepared electrolytes act as a separator and electrolyte at the same time. Therefore, having high mechanical properties is crucial to the application in the LIBs. Mechanical properties were analyzed by tensile stress-strain curves. As shown in Fig. 3d and Table S2, the mechanical strength decreased from 9.5 MPa to 2.1 MPa with the increase in the weight ratio of cellulose from 50 % to 90 %. The elongation at break also decreased from 6.6 to 0.4 %. The reduction of mechanical properties as the increment of cellulose content may be due to the rigid structure of cellulose arising from D-glucose units. In other words, as the cellulose content increases in the blend, the overall flexibility of the material decreases, leading to lower elongation at break. The rigid nature of cellulose also contributes to a reduction in tensile strength, as the material becomes more prone to crack initiation and propagation under stress [27]. In addition, it can be attributed to the enhancement of immiscibility of the two polymers leading to the stress transfer not being carried out properly. This immiscibility increases with higher cellulose content, resulting in poorer stress transfer between the polymer phases. Consequently, the material's ability to withstand tensile forces diminishes, leading to lower mechanical strength. Moreover, the reported modules of blends are in the range of 227.2 MPa–1158.8 MPa.

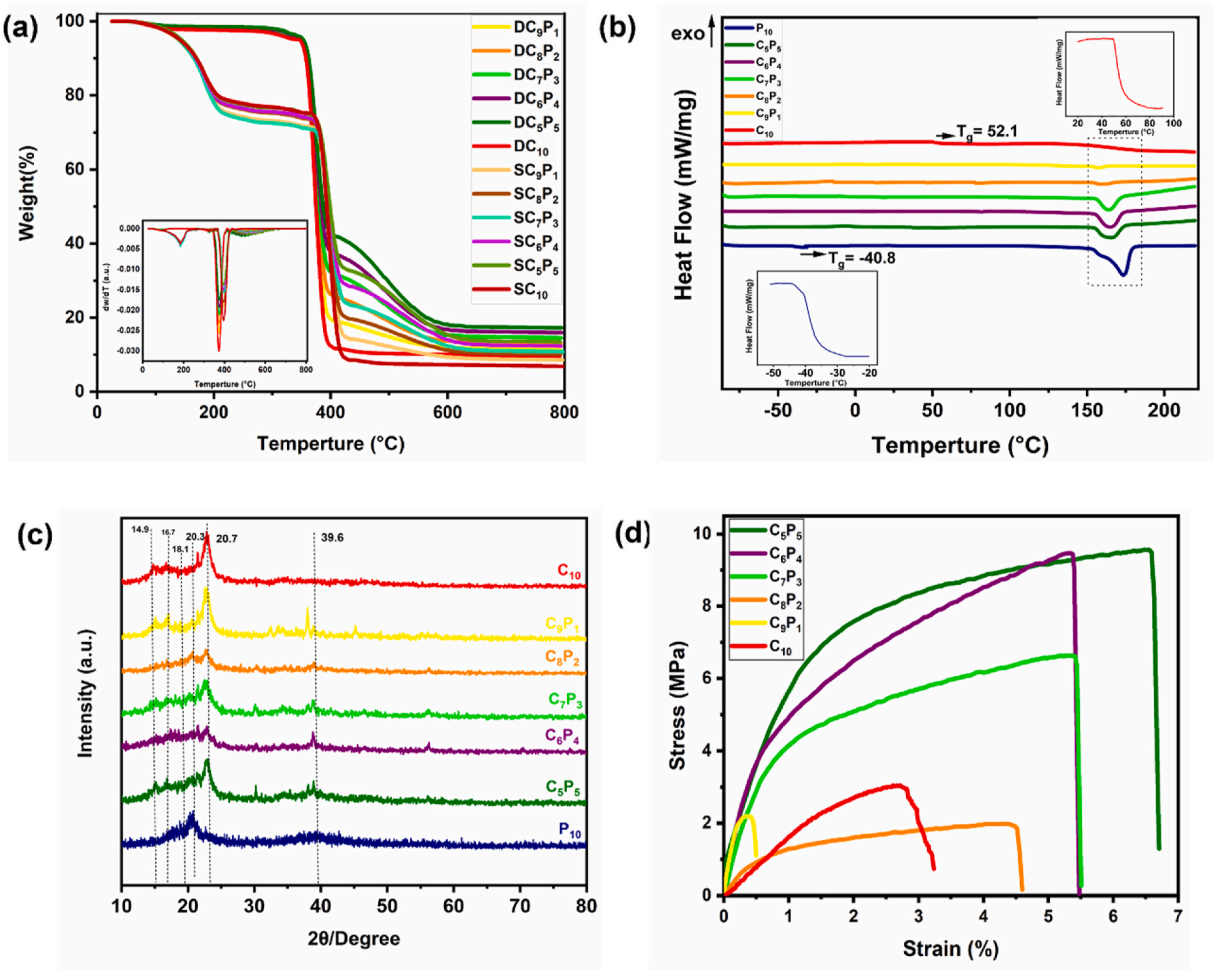

Fig. 3. (a) TGA and DTG curves of prepared polymer electrolytes before and after swelling in salt solution and (b) DSC curves of blend films at different ratios of cellulose/PVDF, (c) XRD patterns of prepared blends by different ratio of cellulose/PVDF, (d) stress-strain behavior of prepared blends by different ratios of cellulose/PVDF.

3.2. Electrochemical properties

The ionic conductivity of the swollen blend films was studied using electrochemical impedance spectroscopy (EIS) (Fig. 4a). Using Zsim software, Nyquist charts have been adapted to the appropriate circuit, resulting in the equivalent circuit depicted in Fig. 4a. In this circuit, R_b represents the electrolyte resistance, C_{SEI} is the capacitance of the solid electrolyte interface (SEI) membrane, and R_{SEI} denotes the resistance of the solid electrolyte interface layer, R_{ct} indicates the charge transfer resistance, $C_{electrode}$ is the electrode capacitance, and W is related to the cation diffusion coefficient [20]. For electrolyte absorption, wettability is a crucial characteristic. Higher wettability boosts the absorption of electrolytes, consequently enhancing the ionic conductivity. Fig. 4b show the absorption of electrolyte. The polar nature of PVDF and cellulose implies electrolyte absorption. According to Fig. 4a and b and Table S3 (Calculated and **)**, cellulose exhibits better wettability and electrolyte absorption with a value of 50.1 %, resulting in an ionic conductivity of 2×10^{-4} S cm^{-1}, while PVDF has low electrolyte absorption, which is equal to 32.5 %, so it shows a lower ionic conductivity of 0.4×10^{-4} S cm^{-1}. In other sides, cellulose has a hydrophilic structure due to the presence of hydroxyl groups, which enhances its interaction with the electrolyte and allows it to absorb more electrolyte compared to the relatively hydrophobic PVDF. This increased absorption provides more pathways for ion transport, resulting in higher ionic conductivity. When the percentage of cellulose in the prepared blend film electrolytes was increased, a corresponding rise in both ionic conductivity and electrolyte absorption was achieved. In sample C_8P_2, the electrolyte adsorption value was 127.5 % and the ionic conductivity was 2.1×10^{-4} S cm^{-1}. In sample C_9P_1 electrolyte absorption was 162 % and the ionic conductivity of 2.3×10^{-4} S cm^{-1} was obtained, which is related to enhancing in wettability. In addition, the high electrolyte absorption and ionic conductivity of these samples can be attributed to the phase separation of these two polymers, and these two samples with the highest interaction parameter values exhibited the most phase separation. Phase separation usually results in the formation of free volume, which serves as a path for ion transport. In this case, the vehicle mechanism is also effective in ion conduction. In samples C_5P_5 and C_6P_4, phase separation presents as dispersed phase

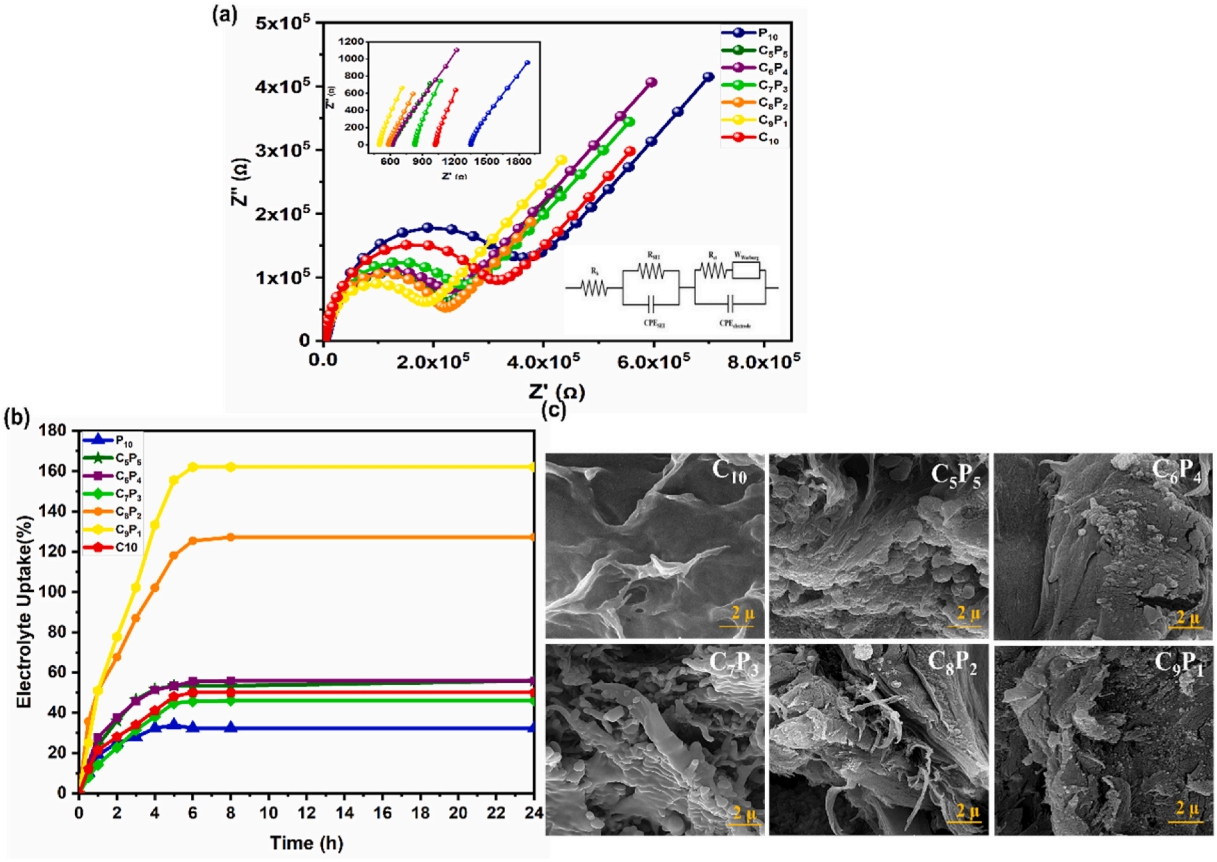

Fig. 4. (a) EIS results of blend films, (b) Swelling ratio of blend films, and (c) Morphology of polymer electrolyte after swelling in salt solution.

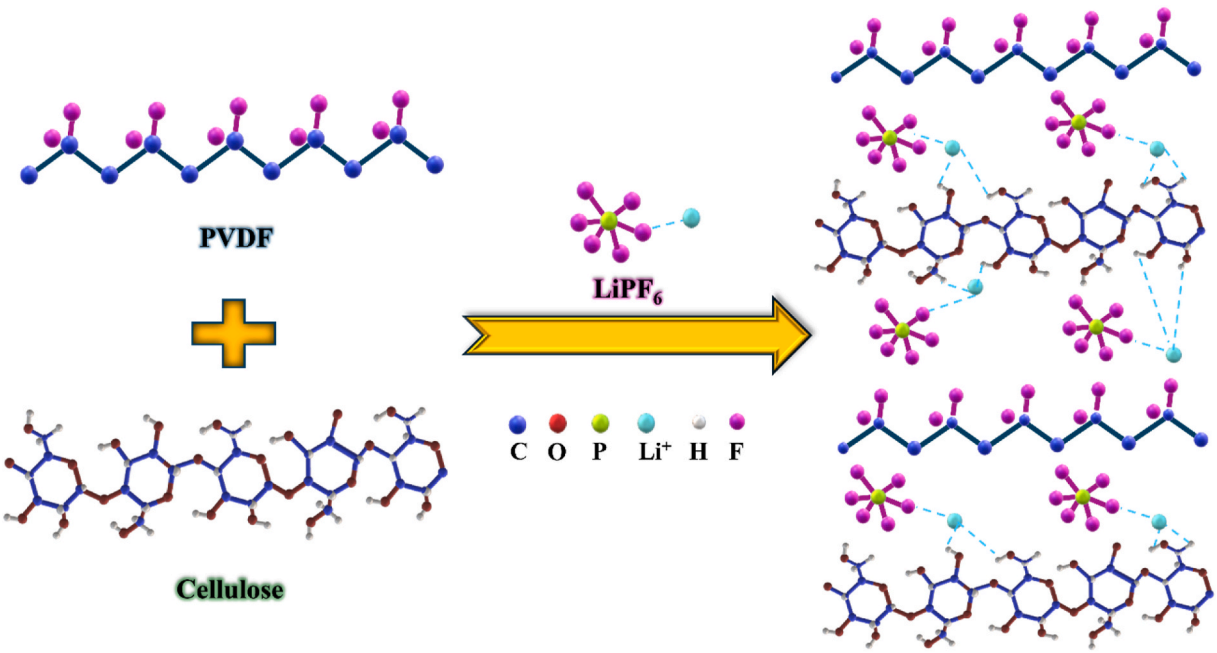

Fig. 5. The cellulose/PVDF blends interactions with the $LiPF_6$ salt.

accumulation with fewer holes and low electrolyte absorption; so, the ion transport by vehicle mechanism has been eliminated. All these reasons led to reduced ionic conductivity. The lowest ionic conductivity with the value of 1.1×10^{-4} S cm^{-1} was obtained for the C_7P_3 sample, indicating that phase separation resulted in less pores and the system has shifted toward a co-continuous morphology. In other words, the C7P3 sample likely represents a transition point in the system, where structural and morphological changes

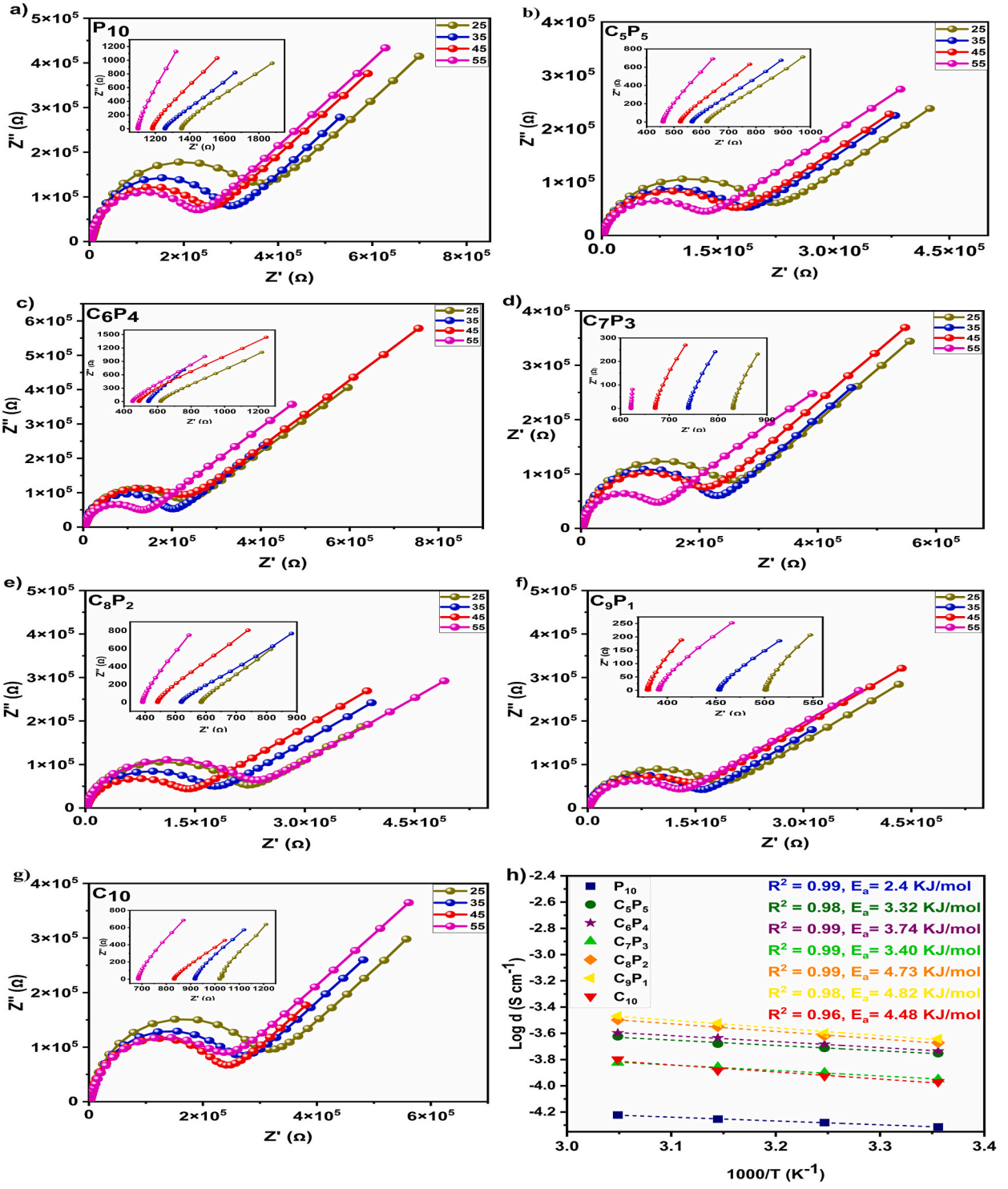

Fig. 6. (a–g) Nyquist curves of cellulose/PVDF blend films according to various temperature, and (h) Arrhenius behavior of prepared polymer electrolytes.

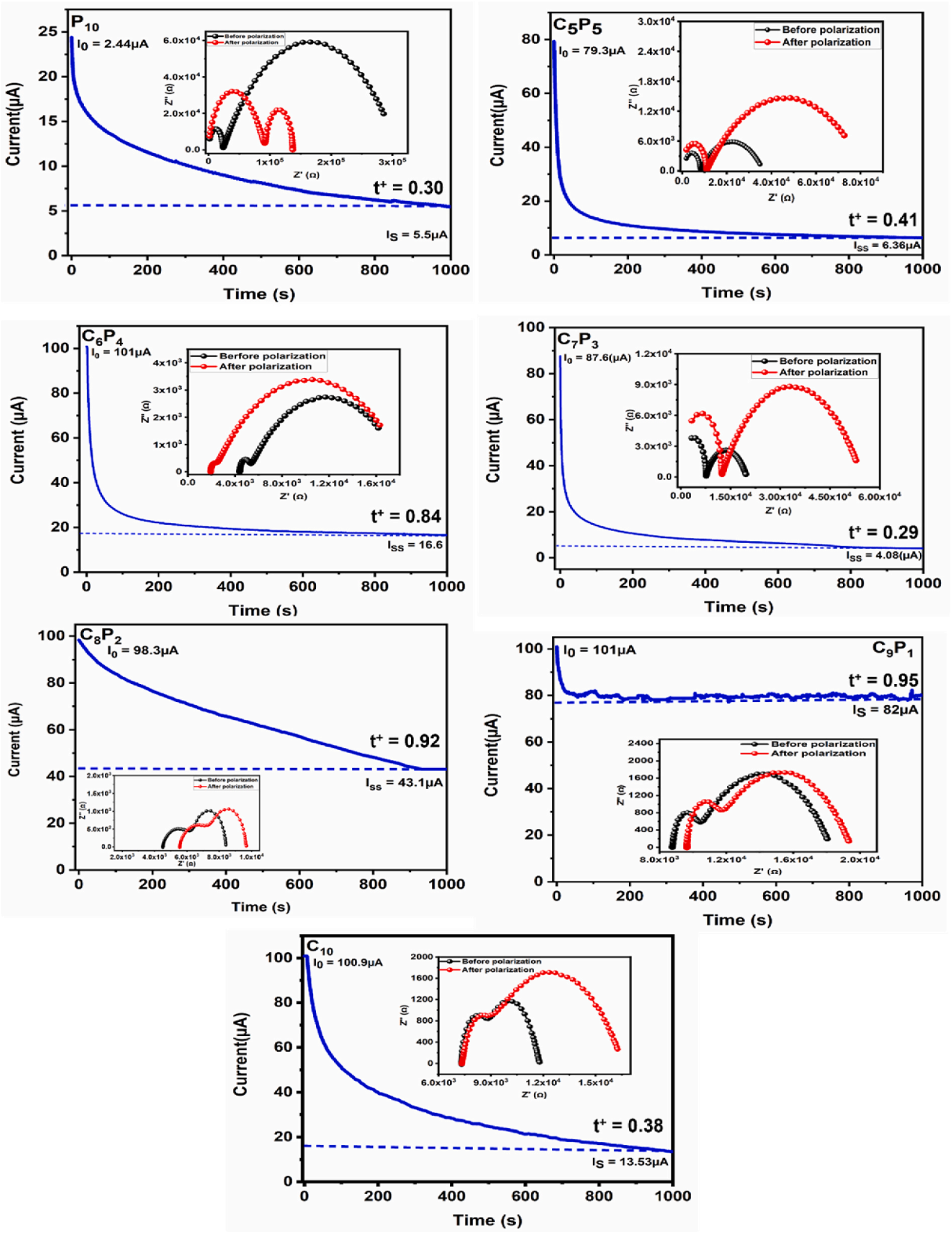

Fig. 7. PVDF/cellulose chronoamperometric curves at room temperature and Nyquist curve before and after polarization.

significantly impact conductivity. At this ratio, the pores may have closed, reducing the pathways available for ion transport and leading to a drop in conductivity. Additionally, the system appears to shift toward a co-continuous morphology, where both cellulose and PVDF form interconnected networks. This transition alters the material's morphology and may hinder the efficient movement of ions, deviating from the expected trend in electrochemical behavior. Furthermore, after swelling, FE-SEM in Fig. 4c revealed that C_9P_1 and C_8P_2 have the most pores, which assist in absorbing and trapping the solvent and provide more free volume for ion transfer, which also affects increasing ion conductivity, whereas C_5P_5, C_6P_4, and C_3P_7 have fewer holes, preventing easy ion movement. All of the results were consistent with the reported electrolyte absorption. To understand the rationale for this distinctive ion conductivity of the synthesized electrolyte, it is necessary to review microstructures of cellulose/PVDF blends interaction by $LiPF_6$ salt (Fig. 5).

The EIS test was carried out in the range of 25–55 °C, in order to investigate the temperature-dependent ionic conductivity, as results are presented in Fig. 6a–g and Table S3. According to the results, there has been an increase in ionic conductivity in response to temperature increase. This phenomenon may be ascribed to the enhanced mobility of polymer chains segmental motion and an increased free volume for ions mobility. The Arrhenius model describes the association between ionic conductivity and temperature. Fig. 6h depicts the fitting of experimental data to the Arrhenius model, and the reported activation energy was calculated using Equation (5):

$$\sigma = \sigma_o \, exp\left(\frac{-E_a}{k_B T}\right) \tag{5}$$

In this equation, E_a indicates activation energy, σ_o represents the pre-exponential factor, k_B indicates the Boltzmann constant, and T is the temperature (K) [28]. Upon increasing the temperature from 25 to 55 °C, the ionic conductivity of C_5P_5 increased from 1.7×10^{-4} to 2.3×10^{-4} S cm^{-1}, and for C_9P_1, it increased from 2.3×10^{-4} to 3.4×10^{-4} S cm^{-1}. This behavior with rising temperature aligns with the typical Arrhenius behavior observed in polymer electrolytes.

The mobility of anions and low diffusion of lithium ions in polymer electrolytes give rise to the concentration polarization and reduction in discharge capacity; therefore, it is essential to determine ion transfer numbers to confirm the cation's mobility. The cation transfer number (t^+) is measured by combined chronoamperometry and EIS before and after a DC polarization (Equation (4)) as results are shown in Fig. 7. All polymer electrolytes showed relatively high t^+ values ($0.41 < t^+ < 0.97$). The functional groups (OH) on the cellulose interact with F atoms in the PF_6 − anions to form H-F hydrogen bonding and hinder the movement of the anions. Also, the interaction between H atoms of PVDF and F atoms in PF_6 − anions restrains the movement of PF_6 $^-$ anions [29]. As the amount of cellulose increases, more hydroxyl groups can be found, resulting in increased interaction with the fluorine atom, whereas lithium transfer is easier in the matrix.

The electrochemical stability window is another crucial property of polymer electrolytes, as shown in Fig. 8. Considering a voltage in the range of 3–3.8 V is required to separate the lithium-ion from the cathode structure, the manufactured polymer electrolytes must have an electrochemical window above 4 V in order to boost charging capacity [30]. This value for all samples was up to 5.5 V. The explanation for the increase in this value when cellulose concentration increases is due to the wrapping more electrolytes. The films are very compatible with carbonate electrolytes, making it suitable for commercial applications without any chemical reactions in lithium-ion batteries.

C_8P_2 and C_9P_1 with the highest values and C_5P_5 having the lowest amount of ionic conductivity and ion transfer number compared to other samples were chosen to investigate charge and discharge performance, and the findings are presented in Fig. 9 and Table S3. Fig. 9a–c illustrate the galvanostatic charge-discharge profiles of GPEs at various C-rates (0.2, 0.5, 1, and 2 C) with voltage ranges of 2.5–5 V. In accordance with the charging capacity amounts, C_9P_1, C_8P_2, and C_5P_5 have initial charge capacities of 219.3, 211.8, and 199.4 mAh g^{-1} at 0.2 C, respectively. Compared to the capacity of the most polymer electrolytes, which is less than 200 mAh g^{-1} at 0.1

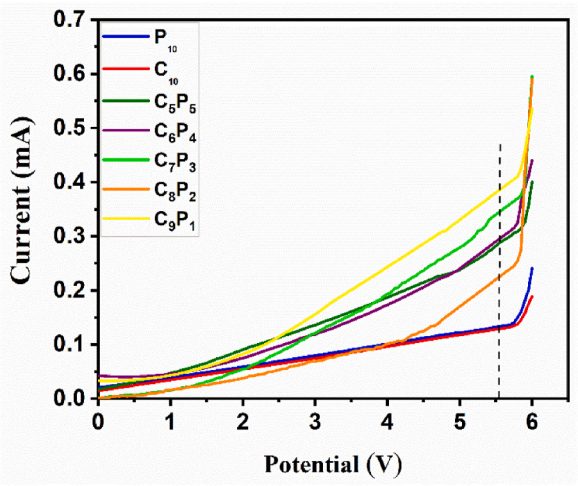

Fig. 8. LSV curves of polymer electrolyte films.

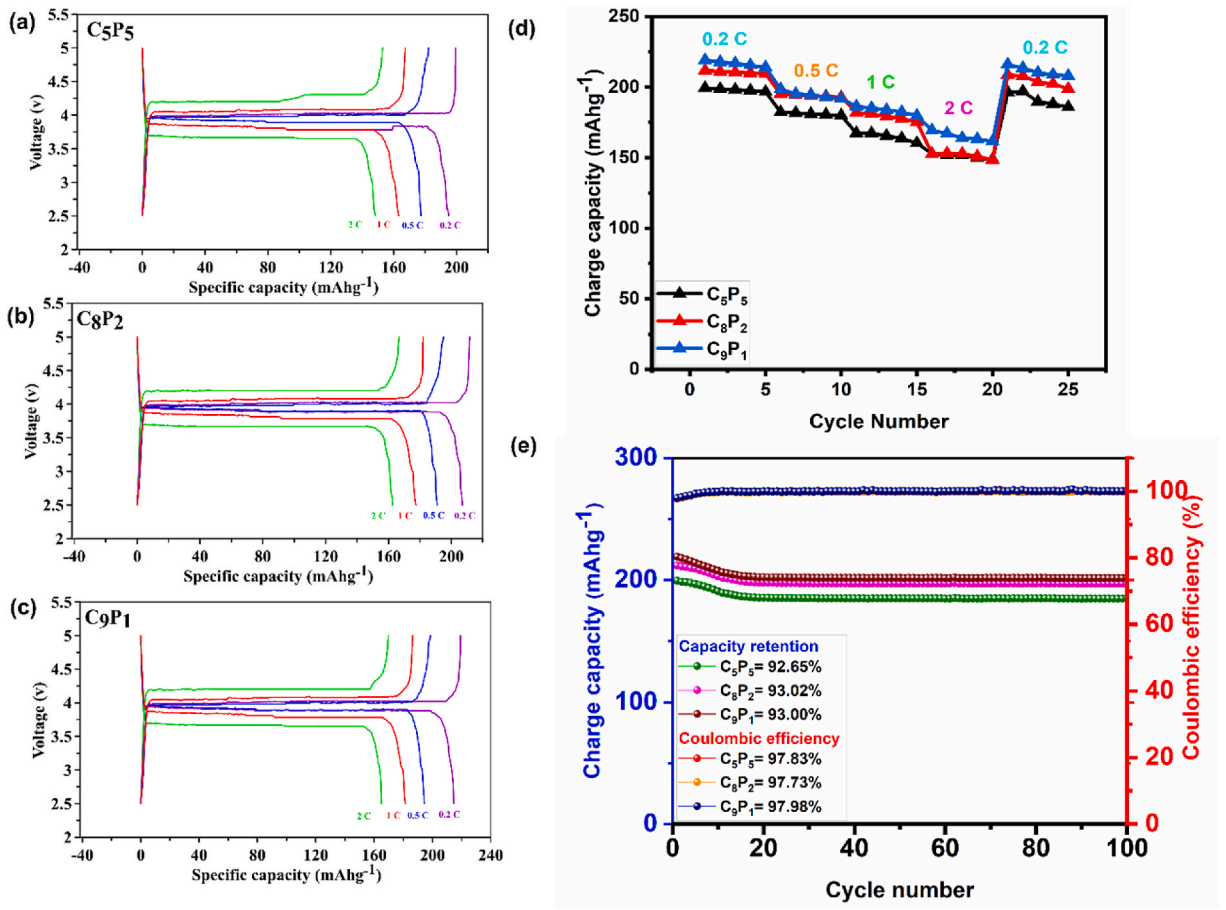

Fig. 9. (a–c) Galvanostatic charge−discharge profiles at different C-rate, (d) rate performance, and (e) discharge capacities and Coulombic efficiency at 0.2 C-rate.

C, these electrolytes have appropriate capabilities [31–33]. The higher capacities observed for C_8P_2 and C_9P_1 compared to C_5P_5 can be ascribed to high ionic conductivity and electrolyte absorption produced by free volume created by phase separation, which offers a platform for efficient transfer and penetration of lithium ions. Furthermore, when current density increased from 0.2 to 2C, charging capacity declined owing to an increase in the polarization effect [34]. Even in this case, acceptable results with 152.8, 166.8, and 169.5 mAh g^{-1} for C_5P_5, C_8P_2, and C_9P_1, respectively have been reported by reaching 2 C. Fig. 9d–e shows the cycling performance and Columbic efficiency (CE) at 0.2C over 100 cycles. C_5P_5 maintains a high capacity of 184.7 mAh g^{-1} after 100 cycles (92.6 % capacity retention). C_8P_2 and C_9P_1 achieved a high capacity of 197 mAh g^{-1} and 201.5 mAh g^{-1} at 100th cycle and capacity retention of 93 % is also obtained for both. The high capacity of these GPEs might be caused by the creation of a stable solid-electrolyte interface layer (SEI). In other words, during the first few charge-discharge cycles, a thin layer of SEI is formed on the electrode surface. The SEI layer functions as a layer of protection, preventing additional electrolyte degradation and preserving the electrode structure, resulting in increased cycle life [35]. Furthermore, the introduction of nanostructured materials (graphite) in electrodes might greatly increase their performance [36].

4. Conclusions

In this research, solution casting has been utilized for producing PVDF/cellulose blend films with varying proportions. Calculated interaction parameter and the resulting morphologies of films demonstrated the immiscibility of the two polymers. The findings revealed that the sample with the highest cellulose content had the most phase separation. The produced polymer gel electrolytes were studied for electrochemical properties. The C_9P_1 sample with maximal phase separation had the highest ionic conductivity (2.3×10^{-4} S/cm), arising from improved free volume and electrolyte absorption. All the blend films had the highest ion transfer number in the range of 0.41–0,95, which was attributed to a decrease in anions' mobility caused by the interaction of the F atoms of PF_6^- salt with the hydrogen atoms of PVDF and the hydroxyl groups of cellulose. The samples have been shown to have an electrochemical stability window above 5.5 V. Furthermore, due to the use of graphite as an anode and its compatibility with the electrolyte, dendritic growth was restricted, resulting in consistent cyclic performance with capacity retention of 92.65 %, 93.02 %, and 93 % for C_5P_5, C_8P_2, and

C_9P_1, respectively, after 100 cycles. The exceptional performance of GPEs makes them good candidates for replacing the traditional liquid electrolytes used in lithium batteries.

CRediT authorship contribution statement

Shirin Mohamadzade: Investigation. **Seyedeh-Arefeh Safavi-Mirmahalleh:** Writing – original draft. **Hossein Roghani-Mamaqani:** Resources. **Mehdi Salami-Kalajahi:** Writing – review & editing, Supervision, Conceptualization.

Data availability

Data will be made available on request.

Funding

This research received grant from Iran National Science Foundation (INSF) with grant number of 4016145.

Declaration of competing interest

The authors declare that they have no known competing financial interests or personal relationships that could have appeared to influence the work reported in this paper.

Appendix A. Supplementary data

Supplementary data to this article can be found online at https://doi.org/10.1016/j.heliyon.2025.e42546.

References

[1] M. Golshan, M. Salami-Kalajahi, Unraveling chromism-induced marvels in energy storage systems, Prog. Mater. Sci. 148 (2025) 101374, https://doi.org/10.1016/j.pmatsci.2024.101374.
[2] T. Kim, W. Song, D.Y. Son, L.K. Ono, Y. Qi, Lithium-ion batteries: outlook on present, future, and hybridized technologies, J. Mater. Chem. A 7 (2019) 2942–2964, https://doi.org/10.1039/C8TA10513H. .
[3] L. Long, S. Wang, M. Xiao, Y. Xiao Xiao, Polymer electrolytes for lithium polymer batteries, J. Mater. Chem. A 4 (2016) 10038–10069, https://doi.org/10.1039/C6TA02621D. .
[4] G. Nagasubramanian, K. Fenton, Reducing Li-ion safety hazards through use of non-flammable solvents and recent work at Sandia National Laboratories, Electrochim. Acta 101 (2013) 3–10, https://doi.org/10.1016/j.electacta.2012.09.065. .
[5] A. Enayati-Gerdroodbar, S.N. Eliseeva, M. Salami-Kalajahi, A review on the effect of nanoparticles/matrix interactions on the battery performance of composite polymer electrolytes, J. Energy Storage 68 (2023) 107836, https://doi.org/10.1016/j.est.2023.107836.
[6] D. Yu, X. Li, J. Xu, Safety regulation of gel electrolytes in electrochemical energy storage devices, Sci. China Mater. 62 (2019) 1556–1573, https://doi.org/10.1007/s40843-019-9475-4. .
[7] M. Salami-Kalajahi, Polymers from Renewable Resources: Energy Storage Applications, Polymers from Renewable Resources, vol. 15, 2024, pp. 397–516, https://doi.org/10.1177/20412479241283844.
[8] A. Song, Y. Huang, B. Liu, H. Cao, X. Zhong, Y. Lin, M. Wang, X. Li, W. Zhong, Gel polymer electrolyte based on polyethylene glycol composite lignocellulose matrix with higher comprehensive performances, Electrochim. Acta 247 (2017) 505–515, https://doi.org/10.1016/j.electacta.2017.07.048. .
[9] S.A. Safavi-Mirmahalleh, S.N. Eliseeva, A.R. Moghaddam, H. Roghani-Mamaqani, M. Salami-Kalajahi, Investigation of the effect of poly[poly (ethylene glycol) methyl ether methacrylate] addition on the electrochemical performance of cellulose-based solid-and gel-polymer electrolytes in lithium-ion batteries, ACS Appl. Energy Mater. 6 (2023) 9624–9636, https://doi.org/10.1021/acsaem.3c01716. .
[10] L. Zhang, H. Gao, G. Jin, S. Liu, J. Wu, H. Wu, S. Wang, Cellulose-based electrolytes for advanced lithium-ion batteries: recent advances and future perspectives, ChemNanoMat 8 (2022) e202200142, https://doi.org/10.1002/cnma.202200142. .
[11] M. Muddasar, A. Beaucamp, M. Culebras, M.N. Collins, Cellulose: characteristics and applications for rechargeable batteries, Int. J. Biol. Macromol. 219 (2022) 788–803, https://doi.org/10.1016/j.ijbiomac.2022.08.026. .
[12] K.S. Ngai, S. Ramesh, K. Ramesh, J.C. Juan, A review of polymer electrolytes: fundamental, approaches and applications, Ionics 22 (2016) 1259–1279, https://doi.org/10.1007/s11581-016-1756-4. .
[13] G. Suresh, G. Mallikarjunachari, S. Jatav, C. Thirmal, M.S. Ramachandra Rao, D.K. Satapathy, Evolution of morphology, ferroelectric, and mechanical properties in poly (vinylidene fluoride)–poly (vinylidene fluoride-trifluoroethylene) blends, J. Appl. Polym. Sci. 135 (2018) 45955, https://doi.org/10.1002/app.45955. .
[14] I. Nicotera, L. Coppola, C. Oliviero, M. Castriota, E. Cazzanelli, Investigation of ionic conduction and mechanical properties of PMMA–PVdF blend-based polymer electrolytes, Solid State Ionics 177 (2006) 581–588, https://doi.org/10.1016/j.ssi.2005.12.028. .
[15] J. Parameswaranpillai, S. Thomas, Y. Grohens, Polymer blends: state of the art, new challenges, and opportunities, Characterization of polymer blends (2014) 1–6.
[16] Y. Wu, Y. Li, Y. Wang, Q. Liu, Q. Chen, M. Chen, Advances and prospects of PVDF based polymer electrolytes, J. Energy Chem. 64 (2022) 62–84, https://doi.org/10.1016/j.jechem.2021.04.007. .
[17] M. Jagan, S.P. Vijayachamundeeswari, A comprehensive investigation of Lithium-based polymer electrolytes, J. Polym. Res. 30 (2023) 250, https://doi.org/10.1007/s10965-023-03623-8. .
[18] M.R. Asghar, Y. Zhang, A. Wu, X. Yan, S. Shen, C. Ke, J. Zhang, Preparation of microporous Cellulose/Poly (vinylidene fluoride-hexafluoropropylene) membrane for lithium ion batteries by phase inversion method, J. Power Sources 379 (2018) 197–205, https://doi.org/10.1016/j.jpowsour.2018.01.052. .
[19] X. Zuo, X. Ma, J. Wu, X. Deng, X. Xiao, J. Liu, J. Nan, Self-supporting ethyl cellulose/poly (vinylidene fluoride) blended gel polymer electrolyte for 5 V high-voltage lithium-ion batteries, Electrochim. Acta 271 (2018) 582–590, https://doi.org/10.1016/j.electacta.2018.03.195. .
[20] M.Y. Zhang, M.X. Li, Z. Chang, Y.F. Wang, J. Gao, Y.S. Zhu, Y.P. Wu, W. Huang, A sandwich PVDF/HEC/PVDF gel polymer electrolyte for lithium ion battery, Electrochim. Acta 245 (2017) 752–759, https://doi.org/10.1016/j.electacta.2017.05.154. .

[21] A.E. Gerdroodbar, H. Alihemmati, S.-A. Safavi-Mirmahaleh, M. Golshan, R. Damircheli, S.N. Eliseeva, M. Salami-Kalajahi, A review on ion transport pathways and coordination chemistry between ions and electrolytes in energy storage devices, J. Energy Storage 74 (2023) 109311, https://doi.org/10.1016/j.est.2023.109311.
[22] P. Dhatarwal, R.J. Sengwa, Polymer compositional ratio-dependent morphology, crystallinity, dielectric dispersion, structural dynamics, and electrical conductivity of PVDF/PEO blend films, Macromol. Res. 27 (2019) 1009–1023, https://doi.org/10.1007/s13233-019-7142-0. .
[23] H. Alihemmati, A. Enayati-Gerdroodbar, M. Golshan, M. Salami-Kalajahi, A fluorescent magnetic nanocrystalline cellulose nanosensor based on rhodamine B for Fe^{3+} ion detection, J. Mol. Liq. 416 (2024) 126536, https://doi.org/10.1016/j.molliq.2024.126536.
[24] P. Singh, H. Borkar, B.P. Singh, V.N. Singh, A. Kumar, Ferroelectric polymer-ceramic composite thick films for energy storage applications, AIP Adv. 4 (2014) 087117, https://doi.org/10.1063/1.4892961. .
[25] S.M.A.S. Keshk, M.S. Hamdy, Preparation and physicochemical characterization of zinc oxide/sodium cellulose composite for food packaging, Turk. J. Chem. 43 (2019) 94–105, https://doi.org/10.3906/kim-1803-83. .
[26] S. Bodkhe, P.S.M. Rajesh, S. Kamle, V. Verma, Beta-phase enhancement in polyvinylidene fluoride through filler addition: comparing cellulose with carbon nanotubes and clay, J. Polym. Res. 21 (2014) 1–11, https://doi.org/10.1007/s10965-014-0434-3. .
[27] S.Y. Xiao, Y.Q. Yang, M.X. Li, F.X. Wang, Z. Chang, Y.P. Wu, X. Liu, A composite membrane based on a biocompatible cellulose as a host of gel polymer electrolyte for lithium ion batteries, J. Power Sources 270 (2014) 53–58, https://doi.org/10.1016/j.jpowsour.2014.07.058. .
[28] S. Liang, W. Yan, X. Wu, Y. Zhang, Y. Zhu, H. Wang, Y. Wu, Gel polymer electrolytes for lithium ion batteries: fabrication, characterization and performance, Solid State Ionics 318 (2018) 2–18, https://doi.org/10.1016/j.ssi.2017.12.023. .
[29] M.R. Asghar, Y. Zhang, A. Wu, X. Yan, S. Shen, C. Ke, J. Zhang, Preparation of microporous Cellulose/Poly (vinylidene fluoride-hexafluoropropylene) membrane for lithium ion batteries by phase inversion method, J. Power Sources 379 (2018) 197–205, https://doi.org/10.1016/j.jpowsour.2018.01.052. .
[30] S. Ghosh, U. Bhattacharjee, S. Bhowmik, D.S.K. Martha, A review on high-capacity and high-voltage cathodes for next-generation lithium-ion batteries, Journal of Energy and Power Technology 4 (2022) 1–77, https://doi.org/10.21926/jept.2201002. .
[31] Y. Kuai, F. Wang, J. Yang, H. Lu, Z. Xu, X. Xu, Y. NuLi, J. Wang, Silica-nanoresin crosslinked composite polymer electrolyte for ambient-temperature all-solid-state lithium batteries, Mater. Chem. Front. 5 (2021) 6502–6511, https://doi.org/10.1039/d1qm00769f.
[32] E. Lizundia, D. Kundu, Advances in natural biopolymer-based electrolytes and separators for battery applications, Adv. Funct. Mater. 31 (2021) 1–29, https://doi.org/10.1002/adfm.202005646.
[33] L. Yue, J. Ma, J. Zhang, J. Zhao, S. Dong, Z. Liu, G. Cui, L. Chen, All solid-state polymer electrolytes for high-performance lithium ion batteries, Energy Storage Mater. 5 (2016) 139–164, https://doi.org/10.1016/j.ensm.2016.07.003.
[34] S. Jamalpour, M. Ghahramani, S.R. Ghaffarian, M. Javanbakht, The effect of poly (hydroxyl ethyl methacrylate) on the performance of PVDF/P (MMA-co-HEMA) hybrid gel polymer electrolytes for lithium ion battery application, Polymer 195 (2020) 122427, https://doi.org/10.1016/j.polymer.2020.122427. .
[35] S.H. Beheshti, M. Javanbakht, H. Omidvar, S. Hosen, A. Hubin, iScience Development, retainment, and assessment of the graphite-electrolyte interphase in Li-ion batteries regarding the functionality of SEI-forming additives, iScience 25 (2022) 103862, https://doi.org/10.1016/j.isci.2022.103862.
[36] H. Zhan, J. Xiao, Z. Nie, X. Li, C. Wang, J.G. Zhang, J. Liu, Nanostructured materials for rechargeable batteries : synthesis , fundamental understanding and limitations, Curr. Opin. Chem. Eng. 2 (2013) 151–159, https://doi.org/10.1016/j.coche.2013.03.007.